



HHS Public Access

Author manuscript

Nat Neurosci. Author manuscript; available in PMC 2018 August 05.

Published in final edited form as:

Nat Neurosci. 2018 March ; 21(3): 424–431. doi:10.1038/s41593-018-0070-z.

Structural tract alterations predict down-stream tau accumulation in amyloid positive older individuals

Heidi I.L. Jacobs^{1,2,3}, Trey Hedden², Aaron P. Schultz^{1,2}, Jorge Sepulcre^{1,2}, Rodrigo D. Perea², Rebecca E. Amariglio^{4,5}, Kathryn V. Papp^{4,5}, Dorene M. Rentz^{4,5}, Reisa A. Sperling^{2,4,5}, and Keith A. Johnson^{1,4,5}

¹Division of Nuclear Medicine and Molecular Imaging, Department of Radiology, Massachusetts General Hospital/Harvard Medical School, Boston, MA ²The Athinoula A. Martinos Center for Biomedical Imaging, Department of Radiology, Massachusetts General Hospital/Harvard Medical School, Boston, MA ³Faculty of Health, Medicine and Life Sciences, School for Mental Health and Neuroscience, Alzheimer Centre Limburg, Maastricht University, Maastricht, The Netherlands ⁴Center for Alzheimer Research and Treatment, Department of Neurology, Brigham and Women's Hospital, Harvard Medical School, Boston, MA ⁵Department of Neurology, Massachusetts General Hospital/Harvard Medical School, Boston, MA

Abstract

Animal models of Alzheimer's disease (AD) have suggested that tau pathology propagation, facilitated by amyloid pathology, may occur along connected pathways. To investigate these ideas in humans, we combined amyloid scans with longitudinal data on white matter connectivity, hippocampal volume, tau positron emission tomography and memory performance in 256 cognitively healthy older individuals. Lower baseline hippocampal volume was associated with increased mean diffusivity of the connecting hippocampal cingulum bundle (HCB). HCB diffusivity predicted tau accumulation in the downstream-connected posterior cingulate cortex (PCC) in amyloid positive, not in amyloid negative individuals. Furthermore, HCB diffusivity predicted memory decline in amyloid positive individuals with high PCC tau binding. Our results provide *in vivo* evidence that higher amyloid pathology strengthens the association between HCB diffusivity and tau accumulation in the down-stream PCC and, facilitates memory decline. This confirms amyloid's crucial role in potentiating neural vulnerability and cognitive decline marking the onset of preclinical AD.

Users may view, print, copy, and download text and data-mine the content in such documents, for the purposes of academic research, subject always to the full Conditions of use: http://www.nature.com/authors/editorial_policies/license.html#terms

Corresponding author: Dr. Heidi Jacobs, PhD, Department of Radiology, Massachusetts General Hospital/Harvard Medical, Boston MA 02114, USA, [hjacobsmgh.harvard.edu](mailto:hjacobs@mgh.harvard.edu).

Author contributions

H.I.L.J. designed the study, analyzed the diffusion and behavioral data, performed statistical analyses and wrote the manuscript. T.H. performed the factor analyses, aided in data interpretation and manuscript preparation. A.P.S. analyzed the PET and structural data and aided in and manuscript preparation. J.S. aided in the connectivity data analysis and manuscript preparation. R.D.P. aided in data analysis and manuscript preparation. R.E.A., K.V.P. and D.M.R. aided in study screening procedures, neuropsychological assessments and manuscript preparations. R.A.S. provided the participants, data analytic tools and aided in study design and manuscript preparations. K.A.J. designed the study, aided in data analyses and interpretation and wrote the manuscript.

Keywords

connectivity; propagation; Tau PET; memory; amyloid; diffusion tensor imaging

Amyloid-beta plaques and tau neurofibrillary tangles, the hallmark lesions of Alzheimer's disease (AD), progress in predictable topographical patterns¹. Amyloid plaques accumulate first in neocortical areas and then in subcortical regions as the disease progresses. Tau neurofibrillary tangles are detected first in the entorhinal cortex and after affecting other medial temporal regions, they spread to other limbic structures and finally to the neocortex^{1,2}. Cognitive functions, especially memory, gradually decline as pathology slowly progresses in load and extent, marking the insidious onset of AD.

Animal studies have provided evidence that the topographical patterns of tau pathology reflect spreading of tau via synaptic connectivity^{3,4}. The highest concentration of normally occurring tau protein is found in the axons of cells, the connections between cells. As axons do not have the required processes to render tau pathology in a fibrillar state, pathological tau remains for a long period of time in the axon allowing these soluble aggregates of the misfolded protein to propagate via axons and cell-to-cell-synaptic transmission⁵⁻⁹. It remains unclear whether, in human disease tau propagation occurs mainly via direct cellular connectivity³ or a combination of connectivity and proximity (regional vulnerability)^{5,6,10}. Notably, amyloid appears to potentiate the propagation of neurofibrillary tangles^{4,11}. Clarification of how tau pathology spreads and the role of amyloid deposition in this process will be key for understanding the pathophysiology of AD and defining new treatment targets.

Motivated by these previous findings, we sought to explore the overarching hypothesis that tau deposition is associated with aberrant structural connectivity under the influence of increased amyloidosis. Additionally, we explored the relevance of these associations for memory in a healthy older population. We combined recently developed Positron Emission Tomography (PET) tracer Flortaucipir (FTP), binding specifically to tau pathology¹²⁻¹⁴, with established diffusion tensor imaging (DTI) methods^{15,16} measuring fiber microstructural properties, and with amyloid PET imaging¹⁷. These methods allowed us to model the untested hypothesis of propagation via connectivity or proximity *in vivo* in humans from an imaging perspective assuming parallels to the biological mechanisms examined in animal studies, albeit on different resolution scales. To that end, we evaluated hypothesized associations (Fig. 1) using longitudinal imaging and memory data from the Harvard Aging Brain Study, an on-going study of cognitively healthy individuals (n=256) followed up to 7 years.

Rationale for investigating limbic pathways in our tau propagation model

Our design is motivated in part by the approach of a recent animal study investigating tau propagation via connectivity or proximity, showing that tau pathology in hippocampal neurons spreads to connected regions and affects the white matter tracts connecting the hippocampus with the distal region³. Figure 1 shows the hypothesized associations investigated consecutively in this study. Histological data suggests that early propagation of

tau pathology occurs from the entorhinal cortex to the hippocampus, via the perforant pathway^{2,18}. As the perforant pathway cannot be captured with the current spatial resolution of DTI, we focused on a fiber tract strongly connected to the hippocampus to explore associations between hippocampal neurodegeneration and tract diffusivity¹⁹. Since the novel tau-tracer FTP was added to the study around year 3–4, we considered variations in hippocampal volume at baseline as a proxy for aging-associated hippocampal tau-related neurodegeneration²⁰. The tract that can be measured reliably and has the most dense connections in the hippocampus is the hippocampal cingulum bundle (HCB)²¹. We predicted that hippocampal volume at baseline would predict abnormal HCB diffusivity over time (orange boxes in Fig 1). Diffusivity of the HCB would in turn be associated with tau accumulation in the down-stream connected posterior cingulate cortex (pink box) and both processes would be associated with memory decline over a six-year period (red box). Recent cross-sectional work from our group suggested that the interaction between amyloid and tau occurs in posterior hippocampal and PCC regions²², supporting the selection of these regions. We additionally included the uncinate fasciculus (UF) as a control tract, since this tract does innervate the medial temporal lobe, but not the hippocampus²³. Furthermore, the UF innervates the prefrontal lobe, a region with limited tau binding in cognitively healthy older individuals. For tau accumulation, we included inferior temporal (IT) tau load as a control measure for spread via proximity versus connectivity. The inferior temporal lobe is spatially proximate to the hippocampus and is does not primarily have connections from the HCB. Finally, using this approach we also investigated the potential moderating role of amyloid in tau propagation and memory decline. Previous postmortem studies have shown that tau pathology in the hippocampus is higher in amyloid positive individuals compared to amyloid negative individuals and that tau pathology outside of the medial temporal lobe in the context of amyloid pathology is associated with increased cognitive decline^{24,25}. We therefore hypothesized that neocortical amyloid deposition (yellow box) is associated with increased hippocampal volume loss and potentiates the effect of abnormal tract diffusivity on increased tau-accumulation in the PCC (Fig. 1).

Results

Participants (n=256) from the Harvard Aging Brain Study²⁶ underwent serial imaging and annual neuropsychological assessments during seven years (Supplementary Figure 1). At baseline, the median age of the participants was 73.5 years (interquartile range [IQR], 68.5 – 78.25 years), their median educational level was 16 years (IQR, 13 – 18 years) and their median Mini-Mental State Examination (MMSE) screening score was 29 points (IQR, 28 – 30). One hundred forty-five participants (60.16%) were female. At baseline, all participants were cognitively healthy as determined by the MMSE, a Clinical Dementia Rating Scale of 0 and age and education adjusted scores on the Logical Memory delayed recall test. All participants underwent a comprehensive medical and neurological evaluation to exclude major psychiatric or neurological disorders (see Online Methods).

Amyloid deposition is associated with increased hippocampal volume loss

We first examined whether smaller hippocampal volume at baseline and volume loss over time (or atrophy) was associated with neocortical amyloid deposition at baseline.

Hippocampal volume, adjusted for intracranial volume, was determined by FreeSurfer²⁷. Amyloid deposition was examined with PET using the Pittsburg B compound (PiB) tracer expressed as the distribution volume ratio (DVR) with cerebellar grey as reference tissue²⁸. Amyloid status was assessed using the cutoff 1.20 (amyloid positive n=61, amyloid negative n=183, missing cases=12) determined by a previous Gaussian mixture modeling approach²⁹ for the total sample for a large cortical ROI aggregate that included frontal, lateral, temporal and retrosplenial cortices (FLR).

Amyloid positive individuals were significantly older and as expected, were more likely to be *APOE-ε4* carrier compared to amyloid negative individuals. No differences were found for sex, education, MMSE or memory scores. Even though amyloid positive individuals showed lower adjusted hippocampal volumes at baseline (Table 1), when correcting for age, sex and education the regression analyses showed no relationship between hippocampal volume and amyloid status at baseline (left hippocampus: $\beta=-85.58$, $t(239)=-1.35$, $p=0.18$ [95% CI: -210.88, 39.72]; right hippocampus: $\beta=-86.85$, $t(239)=-1.54$, $p=0.13$, [95% CI: -197.97, 24.27]).

Longitudinal analyses with linear mixed effect models showed a steeper decline in hippocampal volume in amyloid positive compared to amyloid negative individuals over a 6-year follow-up period (right hippocampus: $\beta=-25.25$, $t(206)=-2.49$, $p=0.014$, [95% CI: -45.26, -5.24]; left hippocampus: $\beta=-17.86$, $t(206)=-2.01$, $p=0.046$, [95% CI: -35.36, -0.35], (453 observations, n=244)). These findings corroborate previous findings from our group and are consistent with disease models suggesting that neurodegeneration occurs downstream of amyloid pathology²⁹. We should note however that tissue volume measures can reflect multiple underlying pathologies contributing to neurodegeneration of which neurofibrillary tangles are the most characteristic of AD. Entorhinal tau and hippocampal volume measured at the nearest time point correlated significantly (left: $r=-0.43$, right: $r=-0.36$ ($p<0.001$), suggesting that hippocampal volume may be a reasonable proxy for early tau pathology

Lower hippocampal volume is associated with white matter abnormalities of the hippocampal cingulum bundle and uncinate fasciculus at baseline

We examined whether there was a relationship between hippocampal volume at baseline with tract diffusivity at baseline. Tract diffusivity was expressed in four metrics: fractional anisotropy (FA), mean diffusivity (MD), axial diffusivity (AxD) and radial diffusivity (RD) using DTI. Using robust regression analyses with age, education and sex as covariates, we observed associations between right and left hippocampal volume and right and left FA, MD and RD of the HCB (n=256) respectively (Supplementary Table 1 and Supplementary Fig. 2). Associations between hippocampal volume and diffusivity of the UF (n=253) were only found for the right hemisphere. These results confirm an association between local volumetric measures and local structural tract properties. Because Braak neurofibrillary tangle (NFT) stage I-II (involvement of entorhinal cortices and hippocampal formation) is present in more than 80% of individuals aged 60 years and older^{18,30}, these associations are likely a reflection of age-related processes, including tau deposition. However, for determining propagation of tau pathology potentially indicative for memory decline as part

of preclinical AD, it will be important to look at tau accumulation in regions associated with later NFT stages, hence the presence of tau lesions in limbic regions.

Hippocampal volume predicts change in diffusion over time of the hippocampal cingulum bundle, not in the uncinate fasciculus

In accordance with our model (Fig. 1), we next assessed the hypothesis that hippocampal volume would predict changes in HCB diffusivity over time, but not in UF diffusivity. To that end, we used linear mixed effects predicting annual change in tract diffusivity with baseline hippocampal volume as predictor. We also investigated whether diffusivity changes and hippocampal volume changes occur simultaneously. Age, education and sex were included as covariates. We report the statistics of the MD component, as this metric is most commonly associated with aging and the earliest episodic memory deficits¹⁵. Statistics for these and the other metrics can be found in the Supplementary data.

Hippocampal volume at baseline predicted a change in HCB diffusivity in such a way that lower hippocampal volume at baseline was associated with more abnormal white matter diffusivity over time (higher MD, AxD, RD). These associations were only significant for the right side (for MD: left: $\beta=-0.0006$, $t(128)=-0.82$, $p=0.417$; right: $\beta=-0.002$, $t(128)=-2.26$, $p=0.025$, 386 observations, Fig. 2, Supplementary Fig. 3). Hippocampal volume did not predict changes in UF diffusivity over time (for MD: left: $\beta=0.001$, $t(123)=0.42$, $p=0.675$; right: $\beta=0.0005$, $t(123)=1.07$, $p=0.283$, 379 observations) (Fig. 2, Supplementary Table 2). Similar relationships were observed when investigating the association between change in hippocampal volume with change in HCB or UF diffusivity (Supplementary Fig. 4). Right hippocampal volume change predicted a change in right HCB MD, no associations were found for the left hemisphere (for MD: left: $\beta=-0.029$, $t(128)=-1.06$, $p=0.29$; right: $\beta=-0.037$, $t(128)=-2.19$, $p=0.03$, 386 observations). No associations were found between change in hippocampal volume and change in UF diffusivity (for MD: left: $\beta=-0.041$, $t(123)=-0.48$, $p=0.63$; right: $\beta=0.004$, $t(123)=0.50$, $p=0.62$, 379 observations) (Supplementary Table 2).

To establish directionality, we also modeled reverse associations, investigating whether baseline or change in white matter diffusivity of these tracts predicted hippocampal volumes changes over time. Baseline or change in HCB or UF diffusivity (left and right) did not predict changes in hippocampal volume over time (Supplementary Table 3).

These results support the hypothesis that hippocampal volume specifically is associated with white matter abnormalities of the HCB and not another nearby tract. Notably, we only found associations for the right hemisphere, even though right hippocampal volume was larger than the left (mean difference=106.11, paired t-test=-6.75, $p<0.001$). Furthermore, we were able to show directionality in these associations.

Hippocampal cingulum diffusivity selectively predicts accumulation of tau pathology in the connected PCC in amyloid-positive individuals

Our previous analyses suggested that hippocampal neurodegenerative processes are associated with structural abnormalities of nearby tracts. However, the question remains whether neurodegenerative-associated connectivity loss predicts increased accumulation in a

region at the anatomic terminus of the HCB. To that end, the linear mixed effects models included annual tau accumulation in the PCC as the outcome measure and white matter diffusivity at baseline as the predictor. Tau accumulation was measured beginning on average 3.01 years (± 0.96) after baseline MRI measurement ($n=141$), with an average follow-up ($n=71$), duration of 2.24 ± 0.49 years. In all models, tau binding was expressed as annual increase (from baseline MRI) in regional binding (with cerebellar grey as reference and corrected for partial volume effects)¹². All models were corrected for age, education and sex. The baseline FTP-subsample ($n=141$) did not differ from the original baseline sample ($n=256$) with respect to age (Welch t-test (279.69): -0.38 , $p=0.70$), education (Welch t-test (289.6): 0.92 , $p=0.36$), sex (Chi-square test: 0.003 , $p=0.95$), MMSE scores (Welch t-test (317.25): 1.23 , $p=0.22$) or PiB-PET levels (Welch t-test (301.36): -0.26 , $p=0.79$). PCC tau binding at baseline was not different between individuals with only baseline data versus those with follow-up data (left: Welch t-test (124.76): -0.45 , $p=0.65$, right: Welch t-test (104.9): -1.25 , $p=0.22$).

Diffusion values (MD, AxD, RD) at baseline of the HCB predicted annual changes in PCC tau for the right hemisphere (MD: $\beta=0.002$, $t(69)=2.55$, $p=0.012$, $n=212$ observations), not the left (MD: $\beta=-0.001$, $t(69)=-0.93$, $p=0.356$, Fig. 3, Supplementary Table 4). These effects did not alter when including baseline hippocampal volume in the model (Right: for MD: $\beta=0.002$, $t(69)=2.47$, $p=0.016$, Left: for MD: $\beta=-0.001$, $t(69)=-0.96$, $p=0.341$). Even though hippocampal volume at baseline by itself did not predict PCC tau accumulation over time (right side: $\beta=-0.00001$, $t(68)=-0.83$, $p=0.409$, left: $\beta=-0.00001$, $t(68)=-0.23$, $p=0.821$), these results provide evidence that HCB diffusivity has a more proximal relationship to PCC tau accumulation over time than does hippocampal volume. Baseline diffusion values of the UF were not associated with accumulation of tau in the PCC (Right: for MD: $\beta=0.001$, $t(68)=0.61$, $p=0.544$, Left: for MD: $\beta=0.001$, $t(68)=1.33$, $p=0.186$, Fig. 3, Supplementary Table 4).

These analyses suggest that tau pathology associated with reduced hippocampal volume affects specific tracts and that more abnormal diffusivity in those tracts is associated with increased tau accumulation in a downstream-connected region. To show that this tau accumulation is specific to the PCC, we ran the same models but with tau binding in the IT cortex as the outcome. As shown in Fig. 3, HCB diffusivity values at baseline did not predict tau accumulation in the IT cortex (Right: for MD: $\beta=0.0004$, $t(69)=0.65$, $p=0.517$, Left: for MD: $\beta=-0.0004$, $t(69)=-0.45$, $p=0.657$; Supplementary Table 5). As tau PET data was acquired later in the study, we were not able to investigate the opposite direction, whether accumulation of PCC tau also has detrimental effects on HCB diffusivity.

We next investigated the role of neocortical amyloid deposition in the propagation of tau via white matter connectivity. Amyloid status was assessed using the cutoff 1.20 ($n=2$ missing for participants who underwent FTP-PET). Baseline amyloid status had no direct effect on tau accumulation in the PCC (left: $\beta=0.01$, $t(69)=0.58$, $p=0.57$; right: $\beta=-0.028$, $t(69)=1.74$, $p=0.086$, 210 observations). We then investigated the three-way interaction “baseline amyloid \times baseline HCB diffusivity \times time” in predicting PCC tau accumulation over time. The three-way interaction (210 observations) was significant for right-sided associations (FA, MD and RD) and not for left-sided associations (Right: for MD: $\beta=0.004$, $t(67)=2.58$,

$p=0.012$, Left: for MD: $\beta=0.001$, $t(67)=0.29$, $p=0.775$, Supplementary Table 6 and Supplementary Fig. 5). The associations between baseline right HCB diffusivity and tau accumulation in the right PCC were only found in amyloid positive individuals (Amyloid positive ($n=36$): MD: $\beta=0.005$, $t(20)=3.35$, $p=0.003$; Amyloid negative ($n=103$): MD: $\beta=0.001$, $t(47)=1.36$, $p=0.179$, Fig. 3).

Together, these results suggest that the mechanism underlying tau propagation from the hippocampus to the PCC is related to reduced diffusivity of a connected white matter fiber bundle, the HCB, and not via a proximate connection. The strength of the association between HCB diffusivity and PCC tau is stronger under higher levels of amyloid pathology.

Memory – tract diffusivity associations are driven by tau pathology

Previous studies have shown that tau pathology outside the medial temporal lobe is closely linked with changes in cognition^{12,14}. Baseline FTP-PET data were classified in two groups: participants with low ($n=93$) or high ($n=48$) PCC tau binding. The cutoff, 1.28 SUV_r, was determined with a Gaussian mixture modeling approach (Supplementary Fig. 6). Running these models with PCC tau binding as a continuous measure led to similar results. Memory performance scores were based on factor scores from the total Harvard Aging Brain Study cohort. We performed linear mixed effects models with baseline HCB diffusivity as the predictor and annual changes in memory performance as the outcome. In the second step we examined the interaction between HCB diffusivity by PCC tau status in predicting memory changes, hypothesizing that memory decline associated with increased HCB diffusivity would be stronger in participants with higher tau levels. As in the previous analyses, tau in the IT cortex was also used as a control region for PCC tau (for the Gaussian mixture model defining the cutoff for IT tau (1.73 SUV_r partial volume-corrected): see Supplementary Fig. 6). In all models, age, education and sex were included as covariates. To investigate cognitive domain specificity, control analyses were performed with an executive composite score based on factor scores from the total cohort.

Left and right HCB diffusivity (lower FA, higher MD and RD) at baseline predicted memory decline (Right: for MD: $\beta=-0.002$, $t(906)=-2.70$, $p=0.007$; Left: for MD: $\beta=-0.003$, $t(906)=-2.56$, $p=0.011$, observations=1167), not executive performance decline (Right: for MD: $\beta=-0.0004$, $t(896)=-0.55$, $p=0.58$; Left: for MD: $\beta=-0.0008$, $t(896)=-0.80$, $p=0.42$, observations=1157). The three-way interaction “HCB diffusivity \times PCC tau status \times time” on memory performance was significant for the right HCB (MD, AxD and RD) and not the left HCB (Right: MD: $\beta=-0.006$, $t(566)=-2.43$, $p=0.015$, Left: MD: $\beta=0.002$, $t(566)=0.73$, $p=0.466$, 714 observations, $n=141$; Supplementary Table 7 and Supplementary Fig. 7). This interaction showed that participants with high PCC tau drive the association between right HCB diffusivity and memory performance over time (high PCC tau ($n=48$, 248 observations): MD: $\beta=-0.006$, $t(195)=-3.20$, $p=0.001$, low PCC tau ($n=93$, 466 observations): MD: $\beta=-0.001$, $t(368)=-0.93$, $p=0.352$; Fig. 4). To show regional specificity, we ran the three-way interaction “HCB diffusivity \times IT tau status \times time” on memory performance and we found no significant association for the right or left HCB (Right MD: $\beta=-0.005$, $t(566)=-1.44$, $p=0.150$, Left: MD: $\beta=0.008$, $t(566)=1.17$, $p=0.241$, 714 observations, $n=141$; Supplementary Table 7

Furthermore, no significant three-way interactions were observed with executive function over time as the outcome measure (For PCC tau: Right: MD: $\beta=-0.001$, $t(563)=0.63$, $p=0.53$, Left: MD: $\beta=0.0004$, $t(563)=0.15$, $p=0.88$, 711 observations, $n=141$, Supplementary Table 8; for IT tau: Right: MD: $\beta=0.0001$, $t(563)=0.03$, $p=0.97$, Left: MD: $\beta=0.002$, $t(563)=0.28$, $p=0.78$, 711 observations, $n=141$, Supplementary Table 8).

We then investigated whether in the group with high PCC tau levels, the association between right HCB diffusivity and memory is larger in amyloid positive compared to amyloid negative individuals (three-way interaction for MD of the right HCB: $\beta=-0.009$, $t(193)=-2.36$, $p=0.019$, 248 observations, $n=48$). Breaking this interaction down confirms that amyloid positive individuals are driving these effects (amyloid positive individuals: $n=18$, observations $n=95$: MD: $\beta=-0.011$, $t(72)=-3.69$, $p=0.0004$; amyloid negative individuals: $n=30$, observations $n=153$: MD: $\beta=-0.002$, $t(118)=-0.59$, $p=0.556$, Fig. 4).

Discussion

A defining feature of AD is the progressive accumulation of amyloid and tau pathology. Current disease models suggest a temporal trajectory in which amyloid pathology initiates a chain of events including the increase in amount and extent of tau pathology³¹. The question of how tau pathology propagates from one region to another is crucial for understanding the pathophysiological mechanisms of AD, but is also important for developing novel therapeutics. Potential mechanisms of tau propagation that have been suggested in histological and animal studies include connectivity, proximity, diffusion along axons and neural activity⁵⁻⁹.

In the present work, we provide for the first time *in vivo* evidence that amyloid pathology - a key determinant in the onset of AD³² accompanies the stronger association between structural alterations of the HCB and accumulation of tau pathology in the down-stream PCC. By combining several established and novel *in vivo* neuroimaging methods, we showed that accumulation of tau pathology in a down-stream connected region is specifically associated with properties of connections of that region and not with other proximate connections, such as the UF. While it is important to recognize that current neuroimaging techniques do not have the resolution to understand the molecular mechanisms of tau propagation, these results are consistent with several animal studies and current disease models^{9,11,33}, and additionally also establish a link to memory decline.

Propagation of tau has been investigated predominantly in animal studies. Several studies have shown a stereotypic increase in tau pathology in a time-dependent manner both locally and distal to regions with synaptic connections³⁻⁵, involving axonal degeneration^{3,9}. Tau propagation has been observed from the tau-infused rodent hippocampus to distal regions such as the olfactory and the retrosplenial cortices^{3,4,33,34}. These observations are consistent with our findings of downstream increased PCC tau (including the retrosplenial cortex) in relation to abnormalities of the connecting HCB, which in turn was associated with lower hippocampal volume at baseline. The fact that hippocampal volume was not directly associated with PCC tau accumulation, suggests that changes in tract diffusivity may be an observation related to the underlying mechanisms mediating the spreading of tau^{3,6,8}. The

fact that these associations showed regional selectivity and were not related to diffusivity of another tract or tau in an adjacent region supports the idea that tau pathology propagates via connectivity³. Since the majority of these findings were found in MD, AxD and RD metrics, hippocampal tau pathology seems to induce disruption of both axons and myelin. Variations in the AxD and RD components need to be interpreted cautiously, as these inferences are largely based on animal studies³⁵. Even though we corrected for partial volume effects, it is possible that hippocampal atrophy may have influenced our results. Future studies should therefore consider acquiring multi-shell sequences, such as NODDI, to increase the specificity of these findings.

We did not find evidence for the reverse association of baseline HCB diffusivity predicting hippocampal volume changes over time, suggesting a biological ordering that fits with the spatiotemporal topography of tau pathology where the hippocampus is affected prior to a tract leaving the medial temporal lobe. It is important to acknowledge that neurodegeneration is a slow process and tau and neurodegeneration may be occurring in parallel, with different magnitudes. Tau propagation may be necessary, but not sufficient for volume loss. Most of the animal studies also found no evidence for tau-induced neurodegeneration, but the animals were on average not very aged^{3,9,36,37}. As for retrograde associations, immunohistochemistry studies have shown evidence for both anterograde cell-to-cell propagation and combined anterograde and retrograde spread of tau to and from the hippocampus and mammillary nuclei, and inconsistencies between our results and these studies may be related to differences in spatial resolution inherent to the methodology.

This is the first study suggesting that changes in tract diffusivity are likely related to the biological mechanisms underlying the association between hippocampal volume and PCC tau accumulation over time. The PCC is an important neuronal hub that displays extensive amyloid deposition in animal studies and human neuroimaging studies^{38–40} and plays a crucial role in spatial learning and memory⁴¹. Animal studies have also suggested propagation from the entorhinal cortex to medial frontal regions or olfactory cortex and thus, this phenomenon is most likely not limited to the hippocampus – PCC connection. Since we investigated cognitively healthy older individuals, the variability in frontal tau binding is limited. Longer follow-up or inclusion of early AD patients will allow extending this model to other brain networks.

Abnormalities of the HCB have been associated with increased amyloid deposition^{38,42}. We found that amyloid is associated with an increased relationship between PCC tau and the HCB, suggesting that amyloid is a crucial part of the chain of events promoting tau spread²² and specifically linked to tau-related memory decline. While the role of amyloid as a driving force for tau propagation to distal regions has been shown in *in vitro* and *in vivo* models^{11,33,34}, the exact molecular mechanism underlying tau propagation and its facilitation by amyloid are still poorly understood⁴³. Hyperphosphorylation^{5,37,44}, is one potential mechanism, as dephosphorylation in animal models has been shown to reduce tau propagation. Whether tau pathology in turn can exacerbate amyloid plaques remains under debate^{11,45}. We did not test this in our study as variability in PiB-PET measures over time is low and requires longer follow-up.

These data do not preclude the possibility that other factors or a combination of factors induce tau propagation¹⁰. Animal studies have also provided evidence for functional spread, where regions that fire synchronously and have higher metabolism are more vulnerable^{4,6,8}. Khan et al. (2014) reported that tau pathology in the MTL in APP/Tau mice led to secondary functional changes in medial parietal regions. Interestingly, neuronal networks with a high load of neurofibrillary tangles can remain functionally intact suggesting that more downstream elements at the axonal or synaptic level may show tau-related defects⁴⁶.

It is important to note that all associations we observed were lateralized to the right. Some degree of asymmetry of tau is common AD pathology⁶. A recent study showed bilateral tau pathology with a stronger involvement of the right hemisphere when comparing cognitively healthy with cognitively impaired individuals⁴⁷. This lateralization may be related to the disease stage, so that in cognitively healthy older individuals tau accumulation in the left hemisphere has not yet crossed the detection threshold. However, it has been shown that asymmetries in amyloid and tau pathology occur and remain stable during disease progression^{48,49}. Alternatively, these right-sided associations may also be specific to the cognitive domain under investigation. Recent work indicated that amyloid-memory (verbal and visuospatial) associations are slightly more right lateralized⁴⁸, and work from our group showed stronger right-side relationships between tau pathology and hypometabolic tempoparietal patterns in amyloid positive individuals⁵⁰. It is also possible that the right-sided effects reflect a selection bias. Left-sided pathology may induce more pronounced cognitive deficits, such as language problems, which would exclude such individuals from our study at baseline. Whether this lateralization is also seen in patients or is associated with other cognitive domains needs to be further examined.

The recent development of FTP-PET tracers allows us to measure and visualize tau pathology *in vivo* for the first time, but as they were recently introduced in the HABS cohort, we did not have this information available at baseline. Therefore, we started our cascade of events with hippocampal volume as a proxy of tau pathology. Hippocampal volume changes can also reflect amyloid deposition or various non-AD related pathological processes, including Lewy-bodies, vascular lesions, hippocampal sclerosis, TDP-43 inclusions and argyrophillic grain disease. Nonetheless, hippocampal atrophy is a common accompaniment to AD-related pathology, especially neurofibrillary degeneration²⁰.

In summary, our findings suggest that amyloid contributes to increased spreading of tau via the HCB, confirming that amyloid is a crucial part of the chain of events leading to increased tau pathology and contributing to tau-related memory decline. Possible upstream molecular mechanisms enabling the spread of tau pathology or how amyloid may potentiate this spread have not been tested with our data and remain an open question. Nonetheless, these findings provide empirical foundations for future work on disease models and suggest that the extent of spreading of tau pathology may be an interesting outcome measure for clinical trials⁴⁴ focused on removal of amyloid plaques in the earliest stages, as amyloid potentiates tau propagation.

Online Methods

Participants

Healthy older individuals from the Harvard Aging Brain Study who underwent 3T Magnetic Resonance Imaging (MRI) including diffusion tensor imaging (DTI) at baseline were included for the present study ($n = 256$, mean age = 74.07 (SD = 6.21)). The Harvard Aging Brain Study is a longitudinal study on aging and Alzheimer's disease (AD)²⁶. Participants undergo annual neuropsychological testing and multiple imaging sessions. Participants were included if they had a global score of 0 on the Clinical Dementia Rating scale⁵¹, a Mini-Mental State Examination score ≥ 25 ⁵² and performed within education-adjusted norms on the Logical Memory delayed recall (>10 for ≥ 16 years of education, > 6 for 8–15 years of education and >4 for <8 years of education). All participants underwent at least one comprehensive medical and neurological evaluation and had no major psychiatric or neurological disorders. Presence of clinical depression (Geriatric Depression Scale below 11/20⁵³) or other psychiatric illnesses, history of alcoholism, drug abuse, head trauma, or a family history of autosomal dominant Alzheimer's disease were exclusion criteria. All behavioral and neuroimaging experiments were performed during daytime. Study protocols were approved by the Partners Human Research Committee at Massachusetts General Hospital, and all participants provided written informed consent. We complied with all ethical regulations.

Structural Magnetic Resonance Imaging

All MR-imaging was performed at the Massachusetts General Hospital, Athinoula A. Martinos Center for Biomedical Imaging on a 3T imaging system (TIM Trio; Siemens) with a 12-channel phased-array head coil. Head motion was controlled with a foam pillow and extendable padded head clamps.

The protocol included a structural T1-weighted volumetric magnetization-prepared rapid-acquisition gradient-echo (MPRAGE) sequence (repetition time (TR) = 2300 ms, echo time (TE) = 2.95 ms, and inversion time = 900 ms, flip angle = 9°; and $1.05 \times 1.05 \times 1.2$ mm resolution). Diffusion weighted images were acquired with a single shot spin echo planar imaging sequence (TR = 8040 ms, TE = 84 ms, flip angle = 90°, field of view = $256 \times 256 \times 128$, voxel size = 2mm isotropic, 30 isotropically distributed diffusion-sensitizing gradients with a b-value of 700 s/mm² and 5 non-diffusion weighted images (b = 0 s/mm²)). Participants were scanned at baseline ($n = 256$) and a second time after an average of 2.82 years ($n = 134$, median follow-up 2.62 years (IQR, 2.51–2.85)).

The diffusion MRI data were processed with ExploreDTI version 4.8.6⁵⁴. Data preprocessing included correction of subject motion, eddy current distortion correction, incorporating the B-matrix rotation to preserve the diffusion gradient orientation information correctly, echo-planar imaging susceptibility correction based on each individual's baseline skull-stripped anatomical image and tensor estimation using the robust non-linear least-squares Restore algorithm. Tracks of interest from the JHU Mori atlas template⁵⁵ were warped to each subject's native space using affine and diffeomorphic elastic registration based on 'elastix'⁵⁶. Fractional Anisotropy (FA), Mean Diffusivity (MD), Axial Diffusivity

(AxD) and Radial Diffusivity (RD) values were extracted from the tracts of interests after thresholding $FA > 0.20$ to exclude partial volume effects. Additionally, tract size was included in our statistical models. Partial volume effects vary with the size of the tract and simulations have shown that this approach can account partially for this contamination⁵⁷. Tracts of interest were the hippocampal cingulum bundle (HCB) and the uncinate fasciculus (UF) was chosen as control tract. In three individuals, the UF could not be estimated accurately due to signal dropout and these individuals were discarded for analyses including this tract. The bootstrapped ($n=500$) intra-class correlation coefficient (ICC) adapted for longitudinal data⁵⁸, demonstrated adequate measurement reliability over time. For the HCB, the ICC was 0.63, 0.66, 0.65 and 0.62 for the MD, FA, AxD and RD components relatively. For the UF, the ICC was 0.81, 0.56, 0.74 and 0.84 for the MD, FA, AxD and RD components relatively.

T1-weighted images were processed using FreeSurfer (FS) version 5.1 using the software package's default, automated reconstruction protocol as described previously^{27,59}. Briefly, each T1-weighted image was subjected to an automated segmentation process involving intensity normalization, skull stripping, segregating left and right hemispheres, removing brainstem and cerebellum, correcting topology defects, defining the borders between grey/white matter and grey/cerebrospinal fluid and parcellating cortical and subcortical areas. Using FS's native visualization toolbox, tkmedit, we visually inspected and, if necessary, edited each image for over- or under-estimation of the gray/white matter boundaries and to identify brain areas erroneously excluded during skull stripping.

Participants received T1-weighted scans at baseline ($n=256$), a second time after on average 2.82 years ($n=157$) and a third time after on average 5.08 years from baseline ($n=53$). The total median follow-up was 2.84 years (IQR, 2.61–4.64). The ICC for hippocampal volume measurements over time was 0.88.

Hippocampal volume was adjusted for the estimated intracranial volume (eTIV) using the following equation²⁹:

$$\text{Adjusted hippocampal volume} = \text{raw hippocampal volume} - b(\text{eTIV} - \text{Mean eTIV}),$$

where b indicates the regression coefficient when hippocampal volume is regressed against eTIV.

PiB–Positron Emission Tomography

Pittsburgh Compound B–positron emission tomography (PiB–PET) was performed at the Massachusetts General Hospital PET facility. Carbon 11–PiB was synthesized using a previously published protocol, and imaging was performed at baseline using a PET system (ECAT EXACT HR+; Siemens). ¹¹C PiB PET was acquired with a 8.5 to 15 mCi bolus injection followed immediately by a 60-minute dynamic acquisition in 69 frames (12 frames \times 15 seconds, 57 frames \times 60 seconds). ¹¹C PiB PET data were expressed as the distribution volume ratio (DVR) with cerebellar grey as reference tissue by using the Logan graphical method applied to data from 40 to 60 minutes after injection²⁸. PiB retention was assessed

using a large cortical ROI aggregate that included frontal, lateral, temporal and retrosplenial cortices (FLR) as described previously^{60,61}. Amyloid status was ascertained by a previously determined cutoff value based on Gaussian mixture modeling approach cutoff value=1.20)²⁹. Based on this cutoff 183 individuals were classified as amyloid negative and 61 as amyloid positive at baseline (for 12 cases there was no baseline PiB-PET measurement). The global PiB-DVR was 1.109 (IQR, 1.063 – 1.202) and the median baseline PiB imaging delay from the first neuropsychological assessment was 0.35 years (IQR, 0.24 – 0.49 years) and from the first MRI scan was 0.003 years (IQR, –0.20 – 0.12).

Flortaucipir (FTP) – Positron Emission Tomography

Fluorine 18-FTP was prepared at MGH with a radiochemical yield of 14±3% and specific activity of 216±60 GBq/μmol at the end of synthesis (60min), and validated for human use⁶². PET images were acquired on a Siemens/CTI (Knoxville, TN) ECAT HR+ scanner (3D mode; 63 image planes; 15.2cm axial field of view; 5.6mm transaxial resolution and 2.4mm slice interval). ¹⁸F FTP was acquired from 80–100 minutes after a 9.0 to 11.0 mCi bolus injection in 4 × 5-minute frames. PET data were reconstructed and attenuation corrected, and each frame was evaluated to verify adequate count statistics and absence of head motion. To evaluate the anatomy of cortical FTP binding, each individual PET data set was rigidly coregistered to the subject's MPRAGE data using SPM8 (Wellcome Department of Cognitive Neurology, Function Imaging Laboratory, London). The FS's ROIs defined by MR as described above were transformed into the PET native space. PET data were partial volume corrected using the Geometrical Transfer Matrix method as implemented in FS⁶³. ¹⁸F FTP specific binding was expressed in FS ROIs, the PCC (FS labels the posterior cingulate/retrosplenial cortex as isthmus) and the IT cortex, as the standardized uptake value ratio (SUVr) using the FS's cerebellar grey ROI as reference. IT and entorhinal tau have so far been investigated more closely than PCC in older individuals. Zero-order Pearson's product-moment correlation coefficients show similar behavior across these measures ($r = 0.58$, $p < 0.001$ for PCC and IT and $r = 0.45$ and $p < 0.001$ for PCC and entorhinal tau). The ICC values showed adequate reliability over time (IT tau ICC= 0.86 and PCC tau ICC 0.77).

As the FTP was only recently developed, FTP-PET was introduced later in the HABS study, on average 3.33±0.77 years after the first neuropsychological assessment, 3.01±0.96 years after the first MRI scan and 2.99±0.83 years after the PIB-PET scan. So far, 141 individuals received a first FTP-PET scan and 71 individuals were followed-up after on average 2.24 years from their first tau PET scan. The median follow-up time for tau-PET was 2.16 years (IQR, 1.95 – 2.53).

Cognitive performance

A memory and an executive function composite score were created based on a factor analysis from the entire HABS cohort ($n = 284$). The memory composite (with factor loading weights between parentheses) included the z-score transformations of the delayed recall scores of the 6-Trial Selective Reminding test⁶⁴ (0.739), the free recall of the Free and Cued Selective Reminding Test (0.605) and the delayed recall of the Logical Memory Test⁶⁵ (0.534). Memory was evaluated annually in HABS and therefore we included 1167 evaluations ($n=256$ at baseline, $n=246$ at year 1, $n=233$ at year 2, $n=194$ at year 3, $n= 157$ at

year 4 and $n=81$ at year 5). The executive function composite included the z-score transformations of the Trail Making Test form B minus A⁶⁶ (0.666), the Letter Number Sequencing test⁶⁷ (0.533) and the phonemic fluency FAS test⁶⁸ (0.622). Executive function was also evaluated annually and at the time of the analyses 1157 observations were included (10 participants did not yet had scores for follow up time point 5). The median follow-up duration was 4.05 years (IQ, 2.91 – 4.96 years).

Experimenters collecting MRI or behavioral data were blind to amyloid status or level of tau binding and experimenters collecting PET data were blind to the behavioral data and MRI results.

Statistical analyses

Statistical analyses were performed using statistical software (R version 3.3.0; <http://www.r-project.org/>). All analyses were done during January 2016 – May 2017. No statistical methods were used to pre-determine sample sizes but our sample sizes are similar to those reported in previous publications^{22,29}.

Group characteristics are represented in median and interquartile range. Differences between amyloid positive and negative individuals were tested with the Welch two-sample t-test to account for unequal variances or with the Chi-square test.

Baseline associations between adjusted hippocampal volume and amyloid status or white matter tract diffusivity (diffusion metrics) were investigated using linear robust regression methods with the Huber-M estimator. Robust regression is a more conservative test compared to linear least-square regression methods, as the resulting models are stout against outliers, which were present in the baseline absolute diffusion data.

Longitudinal analyses were performed with a stepwise hypotheses-driven linear mixed-effects (LME) modeling approach using the maximum likelihood estimation, containing a fixed effect for the predictor of interest, a random intercept for each subject and random slope for time (number of years between baseline and follow-up). For all LME models, we compared the Akaike Information Criteria between models with a random intercept and random slope or only a random intercept using the Log-likelihood ratio test and chose the most parsimonious model. To control for longitudinal changes in voxel selection of tracts, we included analytic weights to the LME models examining diffusion values, weighing the error variance inversely by the tract size⁶⁹. In all LME models, age, sex and education and their interaction with time were included as covariate if $p < 0.10$ (using the Wald t-statistic).

To further examine the hypothesized relationships (Fig. 1), we performed several LME models. We provide the formula for the most complex model (with three-way interactions):

$$\begin{aligned} \text{Outcome}_{ij} = & \beta_1 + \beta_2 \text{Age}_i + \beta_3 \text{Education}_i + \beta_4 \text{Sex}_i + \beta_5 \text{PredictorA}_i + \beta_6 \text{PredictorB}_i + \\ & \beta_7 \text{Time}_{ij} + [\beta_8 \text{Age}_i \times \text{Time}_{ij}] + [\beta_9 \text{Education}_i \times \text{Time}_{ij}] + [\beta_{10} \text{Sex}_i \times \text{Time}_{ij}] + \\ & [\beta_{11} \text{PredictorA}_i \times \text{Time}_{ij}] + [\beta_{12} \text{PredictorB}_i \times \text{Time}_{ij}] + [\beta_{13} \text{PredictorA}_i \times \\ & \text{PredictorB}_i \times \text{Time}_{ij}] + b_{si} \text{Time}_{ij} + b_{1i+\varepsilon_i}, \text{ where } \text{Var}(\varepsilon_{ij}) = \sigma^2 / \text{tract size}_i, \\ & \text{Var}(b_{1i}) = \tau^2_1 \text{ and } \text{Var}(b_{\gamma_i}) = \tau^2_\gamma \text{ and } \text{Cov}(b_{1i}, b_{\gamma_i}) = \rho \times \tau_1 \times \tau_\gamma \end{aligned}$$

Outcome = outcome variable measured over time

Age_i, Education_i, Sex_i=Age, education or sex at baseline testing session

Predictor A/B: variables of interest depending on the investigated model

Time_{ij}=Time at testing session, relative to baseline testing session

b_{1i}=random intercept for each subject

b_{si}=random slope for each subject

τ²₁= variance of the residuals of the random intercept

τ²_σ= variance of the residuals of predicting the random slope

We first investigated differences in annual change in hippocampal volume between amyloid positive and amyloid negative individuals. The second models estimated mean annual change in each DTI metric in each tract predicted by baseline hippocampal volume and its interaction with time. To explore directionality, we also estimated mean annual change in adjusted hippocampal volume predicted by diffusivity of the tracts of interest.

In the next step, we estimated mean annual change in PCC tau predicted by tract diffusivity by time. The time variable reflects annual change in PCC tau since baseline MRI measurements (to check the robustness of our models, we also ran these models with the first tau measurement as baseline, and also within a complete-case design (n=71), these LME's provided similar results). The same model was performed with a control tau region, the IT cortex to establish regional specificity of the findings.

In the fourth step, we examined whether the change in tau predicted by HCB diffusivity was different for amyloid positive versus amyloid negative individuals by adding a three-way interaction in the model (HCB diffusivity at baseline × amyloid status × time).

In the final step, we investigated associations with annual changes in memory performance. First, we investigated whether HCB diffusivity predicted memory performance over time. Associations with executive functioning were investigated as control cognitive measure.

Then we added the interaction with PCC tau binding. The same analyses were performed with IT tau binding as control region.

To ease the interpretation and allow breaking down the model, PCC / IT tau binding was dichotomized in low versus high PCC / IT tau load determined with a Gaussian mixture modeling approach on the baseline data. This approach has been employed previously to classify individuals based on amyloid burden⁷⁰ or overall tau burden⁷¹. This method is

preferred since it is data-driven. Multiple Gaussian distributions were fit to the data (1 to 5 distributions or mixtures, allowing for either equal or unequal variances) and the optimal model was selected by evaluating the Bayesian information criterion, which penalizes models with more parameters) and a bootstrapped (n=5000) sequential likelihood ratio test. The optimal model consisted of two distributions of unequal variance. The probability threshold for belonging to either the low or high tau group was set at 50%, which corresponded at a value of 1.28.

After running the LME with the three-way interaction baseline HCB diffusivity \times PCC tau status \times time, we ran a final model within the group with high PCC tau levels containing the three-way interaction HCB diffusivity \times amyloid status \times time. Residual plots and Q-Q-plots were examined for all models. All p-values were two-sided and no correction for multiple comparisons was performed (for each analyses, we performed 4 models for each diffusion metric and for diffusion - hippocampal volume cross-sectional and longitudinal associations: 4 comparisons were performed for the tract of interest and 4 for the control tract per side and per diffusion metric; for the association between tau and diffusion: a total of 3 comparisons were performed for the tract of interest and control region per side and per diffusion metric; for the cognitive analyses: a total of 3 comparisons were performed per cognitive measure, per side and per diffusion metric).

Data availability

Relevant data that support the findings of this study are available from the authors upon reasonable request.

Baseline data from the Harvard Aging Brain Study are also publicly available online: (<http://nmr.mgh.harvard.edu/lab/harvardagingbrain/data>)²⁶. Follow-up data of the Harvard Aging Brain Study is expected to be released in the upcoming year.

Supplementary Material

Refer to Web version on PubMed Central for supplementary material.

Acknowledgments

This work was supported in part by the Athinoula A. Martinos Center for Biomedical Imaging, P41 EEB015896 and shared instrumentation grants S10RR021110, S10OD010364, S10RR023401, S10RR023043 and S10RR019307. The research was supported in major part by the Harvard Aging Brain Study (P01 AG036694). We would like to thank all the participants of the Harvard Aging Brain Study

Competing financial interests

H. Jacobs received funding from Alzheimer Nederland [WE.15-2014-06]. T. Hedden received funding from NIH grant K01 AG040197, P01 AG036694, P50 AG005134, R01 AG053509 and R01 AG034556. A. Schultz has been a paid consultant for Janssen Pharmaceuticals and Biogen. J. Sepulcre received funding from NIH grant K23EB019023. K. Papp is funded by NIA grant K23 AG053422-01 and the Alzheimer's Association, and has served as a paid consultant for Biogen. D. Rentz has done consulting for Eli Lilly and served on the Scientific Advisory Board for Neurotrack. K. Johnson has served as paid consultant for Bayer, GE Healthcare, Janssen Alzheimer's Immunotherapy, Siemens Medical Solutions, Genzyme, Novartis, Biogen, Roche, ISIS Pharma, AZTherapy, GEHC, Lundberg, and Abbvie. He is a site co-investigator for Lilly/Avid, Janssen Immunotherapy and Pfizer. K. Johnson received funding from NIH grants R01 EB014894, R21 AG038994, R01 AG026484, R01 AG034556, P50 AG00513421, U19 AG10483, P01 AG036694, R13 AG042201174210, R01 AG027435 and R01 AG037497 and the Alzheimer's Association grant ZEN-10-174210. R. Sperling has served as a paid consultant for

Abbvie, Biogen, Bracket, Genentech, Lundbeck, Roche, and Sanofi. She has served as co-investigator for Avid, Eli Lilly, and Janssen Alzheimer Immunotherapy clinical trials. She has spoken at symposia sponsored by Eli Lilly, Biogen, and Janssen. R. Sperling receives research support from Janssen Pharmaceuticals, and Eli Lilly and Co. These relationships are not related to the content in the manuscript. She also receives research support from the following grant: P01 AG036694, U01 AG032438, U01 AG024904, R01 AG037497, R01 AG034556, K24 AG0350007, P50 AG005134, U19 AG010483, R01 AG027435, Fidelity Biosciences, Harvard NeuroDiscovery Center, and the Alzheimer's Association

References

1. Braak H, Braak E. Neuropathological staging of Alzheimer-related changes. *Acta Neuropathol.* 1991; 82:239–259. [PubMed: 1759558]
2. Braak H, Braak E. Development of Alzheimer-related neurofibrillary changes in the neocortex inversely recapitulates cortical myelogenesis. *Acta Neuropathol.* 1996; 92:197–201. [PubMed: 8841666]
3. Ahmed Z, et al. A novel in vivo model of tau propagation with rapid and progressive neurofibrillary tangle pathology: the pattern of spread is determined by connectivity, not proximity. *Acta Neuropathol.* 2014; 127:667–683. [PubMed: 24531916]
4. Khan UA, et al. Molecular drivers and cortical spread of lateral entorhinal cortex dysfunction in preclinical Alzheimer's disease. *Nat. Neurosci.* 2014; 17:304–311. [PubMed: 24362760]
5. Hu W, et al. Hyperphosphorylation determines both the spread and the morphology of tau pathology. *Alzheimers Dement.* 2016; 12:1066–1077. [PubMed: 27133892]
6. Lewis J, Dickson DW. Propagation of tau pathology: hypotheses, discoveries, and yet unresolved questions from experimental and human brain studies. *Acta Neuropathol.* 2016; 131:27–48. [PubMed: 26576562]
7. Braak H, Del Tredici K. Alzheimer's pathogenesis: is there neuron-to-neuron propagation? *Acta Neuropathol.* 2011; 121:589–595. [PubMed: 21516512]
8. Wu JW, et al. Neuronal activity enhances tau propagation and tau pathology in vivo. *Nat. Neurosci.* 2016; 19:1085–1092. [PubMed: 27322420]
9. de Calignon A, et al. Propagation of tau pathology in a model of early Alzheimer's disease. *Neuron.* 2012; 73:685–697. [PubMed: 22365544]
10. Walsh DM, Selkoe DJ. A critical appraisal of the pathogenic protein spread hypothesis of neurodegeneration. *Nat. Rev. Neurosci.* 2016; 17:251–260. [PubMed: 26988744]
11. Pooler AM, et al. Amyloid accelerates tau propagation and toxicity in a model of early Alzheimer's disease. *Acta Neuropathol. Commun.* 2015; 3:14. [PubMed: 25853174]
12. Johnson KA, et al. Tau positron emission tomographic imaging in aging and early Alzheimer disease. *Ann. Neurol.* 2016; 79:110–119. [PubMed: 26505746]
13. Marquie M, et al. Validating novel tau positron emission tomography tracer [F-18]-AV-1451 (T807) on postmortem brain tissue. *Ann. Neurol.* 2015; 78:787–800. [PubMed: 26344059]
14. Scholl M, et al. PET Imaging of Tau Deposition in the Aging Human Brain. *Neuron.* 2016; 89:971–982. [PubMed: 26938442]
15. Madden DJ, Bennett IJ, Song AW. Cerebral white matter integrity and cognitive aging: contributions from diffusion tensor imaging. *Neuropsychol. Rev.* 2009; 19:415–435. [PubMed: 19705281]
16. Jones DK, Leemans A. Diffusion tensor imaging. *Methods Mol. Biol.* 2011; 711:127–144. [PubMed: 21279600]
17. Klunk WE, et al. Imaging brain amyloid in Alzheimer's disease with Pittsburgh Compound-B. *Ann. Neurol.* 2004; 55:306–319. [PubMed: 14991808]
18. Braak H, Del Tredici K. The preclinical phase of the pathological process underlying sporadic Alzheimer's disease. *Brain.* 2015; 138:2814–2833. [PubMed: 26283673]
19. Villain N, et al. Sequential relationships between grey matter and white matter atrophy and brain metabolic abnormalities in early Alzheimer's disease. *Brain.* 2010; 133:3301–3314. [PubMed: 20688814]
20. Jicha GA, et al. Neuropathologic outcome of mild cognitive impairment following progression to clinical dementia. *Arch. Neurol.* 2006; 63:674–681. [PubMed: 16682537]

21. Heilbronner SR, Haber SN. Frontal cortical and subcortical projections provide a basis for segmenting the cingulum bundle: implications for neuroimaging and psychiatric disorders. *J. Neurosci.* 2014; 34:10041–10054. [PubMed: 25057206]
22. Sepulcre J, et al. In Vivo Tau, Amyloid, and Gray Matter Profiles in the Aging Brain. *J. Neurosci.* 2016; 36:7364–7374. [PubMed: 27413148]
23. Von Der Heide RJ, Skipper LM, Klobusicky E, Olson IR. Dissecting the uncinate fasciculus: disorders, controversies and a hypothesis. *Brain.* 2013; 136:1692–1707. [PubMed: 23649697]
24. Price JL, Morris JC. Tangles and plaques in nondemented aging and "preclinical" Alzheimer's disease. *Ann. Neurol.* 1999; 45:358–368. [PubMed: 10072051]
25. Delacourte A, et al. Tau aggregation in the hippocampal formation: an ageing or a pathological process? *Exp. Gerontol.* 2002; 37:1291–1296. [PubMed: 12470843]
26. Dagley A, et al. Harvard Aging Brain Study: Dataset and accessibility. *Neuroimage.* 2017; 144:255–258. [PubMed: 25843019]
27. Fischl B, Sereno MI, Dale AM. Cortical surface-based analysis. II: Inflation, flattening, and a surface-based coordinate system. *Neuroimage.* 1999; 9:195–207. [PubMed: 9931269]
28. Logan J, et al. Graphical analysis of reversible radioligand binding from time-activity measurements applied to [N-11C-methyl]-(-)-cocaine PET studies in human subjects. *J. Cereb. Blood Flow Metab.* 1990; 10:740–747. [PubMed: 2384545]
29. Mormino EC, et al. Synergistic effect of beta-amyloid and neurodegeneration on cognitive decline in clinically normal individuals. *JAMA Neurol.* 2014; 71:1379–1385. [PubMed: 25222039]
30. Braak H, Braak E. Frequency of stages of Alzheimer-related lesions in different age categories. *Neurobiol. Aging.* 1997; 18:351–357. [PubMed: 9330961]
31. Hyman BT. Amyloid-dependent and amyloid-independent stages of Alzheimer disease. *Arch. Neurol.* 2011; 68:1062–1064. [PubMed: 21482918]
32. Hardy J, Selkoe DJ. The amyloid hypothesis of Alzheimer's disease: progress and problems on the road to therapeutics. *Science.* 2002; 297:353–356. [PubMed: 12130773]
33. Gotz J, Chen F, van Dorpe J, Nitsch RM. Formation of neurofibrillary tangles in P3011 tau transgenic mice induced by Abeta 42 fibrils. *Science.* 2001; 293:1491–1495. [PubMed: 11520988]
34. Lewis J, et al. Enhanced neurofibrillary degeneration in transgenic mice expressing mutant tau and APP. *Science.* 2001; 293:1487–1491. [PubMed: 11520987]
35. Wheeler-Kingshott CA, Cercignani M. About "axial" and "radial" diffusivities. *Magn. Reson. Med.* 2009; 61:1255–1260. [PubMed: 19253405]
36. Clavaguera F, et al. Transmission and spreading of tauopathy in transgenic mouse brain. *Nat. Cell Biol.* 2009; 11:909–913. [PubMed: 19503072]
37. Takeda S, et al. Neuronal uptake and propagation of a rare phosphorylated high-molecular-weight tau derived from Alzheimer's disease brain. *Nat. Commun.* 2015; 6:8490. [PubMed: 26458742]
38. Harris JA, et al. Transsynaptic progression of amyloid-beta-induced neuronal dysfunction within the entorhinal-hippocampal network. *Neuron.* 2010; 68:428–441. [PubMed: 21040845]
39. Buckner RL, et al. Cortical hubs revealed by intrinsic functional connectivity: mapping, assessment of stability, and relation to Alzheimer's disease. *J. Neurosci.* 2009; 29:1860–1873. [PubMed: 19211893]
40. Dillen KN, et al. Aberrant functional connectivity differentiates retrosplenial cortex from posterior cingulate cortex in prodromal Alzheimer's disease. *Neurobiol. Aging.* 2016; 44:114–126. [PubMed: 27318139]
41. Vann SD, Aggleton JP, Maguire EA. What does the retrosplenial cortex do? *Nat. Rev. Neurosci.* 2009; 10:792–802. [PubMed: 19812579]
42. Rieckmann A, et al. Accelerated decline in white matter integrity in clinically normal individuals at risk for Alzheimer's disease. *Neurobiol. Aging.* 2016; 42:177–188. [PubMed: 27143434]
43. Stancu IC, Vasconcelos B, Terwel D, Dewachter I. Models of beta-amyloid induced Tau-pathology: the long and "folded" road to understand the mechanism. *Mol. Neurodegener.* 2014; 9:51. [PubMed: 25407337]
44. Iqbal K, Liu F, Gong CX. Tau and neurodegenerative disease: the story so far. *Nat. Rev.* 2016; 12:15–27.

45. Hurtado DE, et al. A β accelerates the spatiotemporal progression of tau pathology and augments tau amyloidosis in an Alzheimer mouse model. *Am. J. Pathol.* 2010; 177:1977–1988. [PubMed: 20802182]
46. Kuchibhotla KV, et al. Neurofibrillary tangle-bearing neurons are functionally integrated in cortical circuits in vivo. *Proc. Natl. Acad. Sci. U.S.A.* 2014; 111:510–514. [PubMed: 24368848]
47. Gordon BA, et al. The relationship between cerebrospinal fluid markers of Alzheimer pathology and positron emission tomography tau imaging. *Brain.* 2016; 139:2249–2260. [PubMed: 27286736]
48. Frings L, et al. Asymmetries of amyloid-beta burden and neuronal dysfunction are positively correlated in Alzheimer's disease. *Brain.* 2015; 138:3089–3099. [PubMed: 26280595]
49. Stefanits H, Budka H, Kovacs GG. Asymmetry of neurodegenerative disease-related pathologies: a cautionary note. *Acta Neuropathol.* 2012; 123:449–452. [PubMed: 22222584]
50. Hanseeuw BJ, et al. Fluorodeoxyglucose metabolism associated with tau-amyloid interaction predicts memory decline. *Ann. Neurol.* 2017; 81:583–596. [PubMed: 28253546]
51. Morris JC. The Clinical Dementia Rating (CDR): current version and scoring rules. *Neurology.* 1993; 43:2412–2414.
52. Folstein MF, Folstein SE, McHugh PR. "Mini-mental state". A practical method for grading the cognitive state of patients for the clinician. *J. Psychiat. Res.* 1975; 12:189–198. [PubMed: 1202204]
53. Sheikh, J., Yesavage, J. Geriatric Depression Scale (GDS): recent evidence and development of a shorter version. in: In: Brink, TL., editor. *Clinical Gerontology: A Guide to Assessment and Intervention.* Haworth Press; New York: 1986. p. 165-173.
54. Leemans, A., Jeurissen, B., Sijbers, J., Jones, DK. 17th Annual Meeting of Intl. Soc. Mag. Reson. Med. Hawaii, USA: 2009. Explore DTI: a graphical toolbox for processing, analyzing, and visualizing diffusion MR data. in: p. 3537
55. Mori S, et al. Stereotaxic white matter atlas based on diffusion tensor imaging in an ICBM template. *Neuroimage.* 2008; 40:570–582. [PubMed: 18255316]
56. Klein A, et al. Evaluation of 14 nonlinear deformation algorithms applied to human brain MRI registration. *Neuroimage.* 2009; 46:786–802. [PubMed: 19195496]
57. Vos SB, Jones DK, Viergever MA, Leemans A. Partial volume effect as a hidden covariate in DTI analyses. *Neuroimage.* 2011; 55:1566–1576. [PubMed: 21262366]
58. Nakagawa S, Schielzeth H. Repeatability for Gaussian and non-Gaussian data: a practical guide for biologists. *Biol. Rev. Camb. Philos. Soc.* 2010; 85:935–956. [PubMed: 20569253]
59. Dale AM, Fischl B, Sereno MI. Cortical surface-based analysis. I. Segmentation and surface reconstruction. *Neuroimage.* 1999; 9:179–194. [PubMed: 9931268]
60. Hedden T, et al. Disruption of functional connectivity in clinically normal older adults harboring amyloid burden. *J. Neurosci.* 2009; 29:12686–12694. [PubMed: 19812343]
61. Amariglio RE, et al. Subjective cognitive complaints and amyloid burden in cognitively normal older individuals. *Neuropsychologia.* 2012; 50:2880–2886. [PubMed: 22940426]
62. Shoup TM, et al. A concise radiosynthesis of the tau radiopharmaceutical, [(18)F]T807. *J. Labelled Comp. Radiopharm.* 2013; 56:736–740. [PubMed: 24339014]
63. Greve DN, et al. Cortical surface-based analysis reduces bias and variance in kinetic modeling of brain PET data. *Neuroimage.* 2014; 92:225–236. [PubMed: 24361666]
64. Masur DM, et al. Distinguishing normal and demented elderly with the selective reminding test. *J. Clin. Exp. Neuropsychol.* 1989; 11:615–630. [PubMed: 2808653]
65. Wechsler, DS. Wechsler Memory Scale-Revised. Psychological-Corp; San Antonio, TX: 1987.
66. Wechsler, DS. WAIS-III, Wechsler Adult Intelligence Scale—Third Edition, Administration and Scoring Manual. The Psychological Corporation; New York: 1997.
67. Reitan, RM. Manual for administration of neuropsychological test batteries for adults and children. Reitan Neuropsychology Laboratories; Tucson, AZ: 1979.
68. Benton, AL. Contributions to Neuropsychological Assessment: A Clinical Manual. Oxford University Press; New York: 1983.

69. Domen P, et al. Differential Time Course of Microstructural White Matter in Patients With Psychotic Disorder and Individuals at Risk: A 3-Year Follow-up Study. *Schizophr. Bull.* 2017; 43:160–170. [PubMed: 27190279]
70. Mormino EC, et al. Amyloid and APOE epsilon4 interact to influence short-term decline in preclinical Alzheimer disease. *Neurology.* 2014; 82:1760–1767. [PubMed: 24748674]
71. Wang L, et al. Evaluation of Tau Imaging in Staging Alzheimer Disease and Revealing Interactions Between beta-Amyloid and Tauopathy. *JAMA Neurol.* 2016; 73:1070–1077. [PubMed: 27454922]

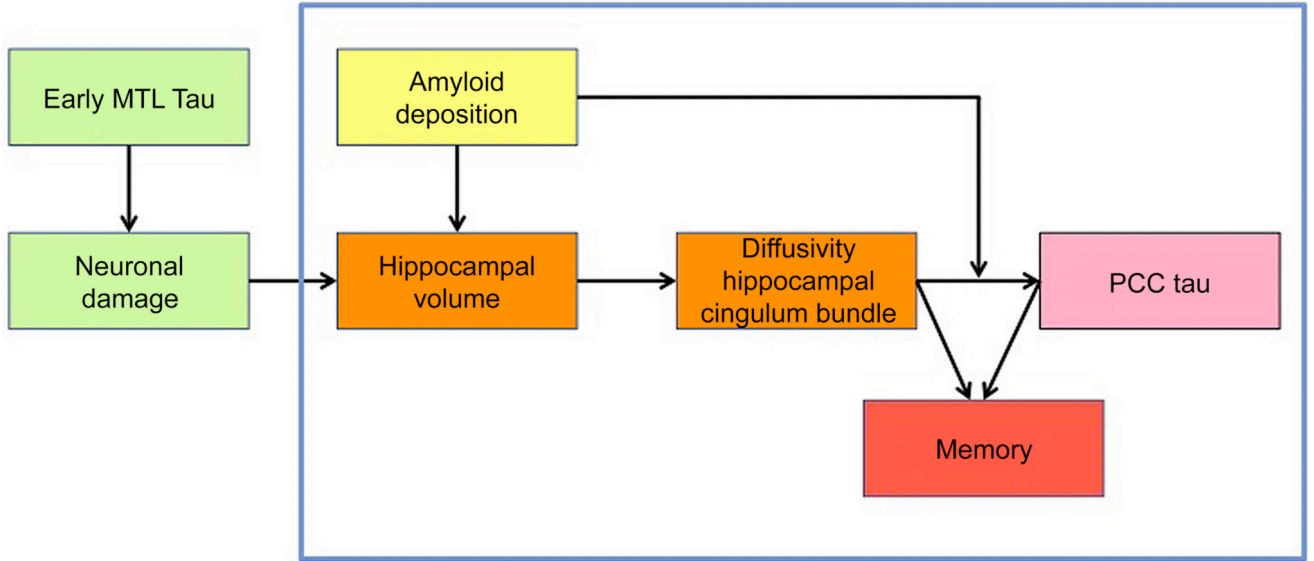


Figure 1. The hypothesized model motivating our design and analyses

The relationships that were specifically analyzed in the current manuscript are within the blue box. The green boxes hypothesize that hippocampal volume loss is resulting from neuronal damage, partially due to early tau pathology in the medial temporal lobe. As tau PET was acquired later in the study and thus this information was not available at baseline, we could not examine the green boxes. The relationship between hippocampal volume and diffusivity of the hippocampal cingulum bundle was analyzed using both baseline measures of hippocampal volume and change in hippocampal volume over time. Abbreviations: MTL = medial temporal lobe, PCC = posterior cingulate cortex.

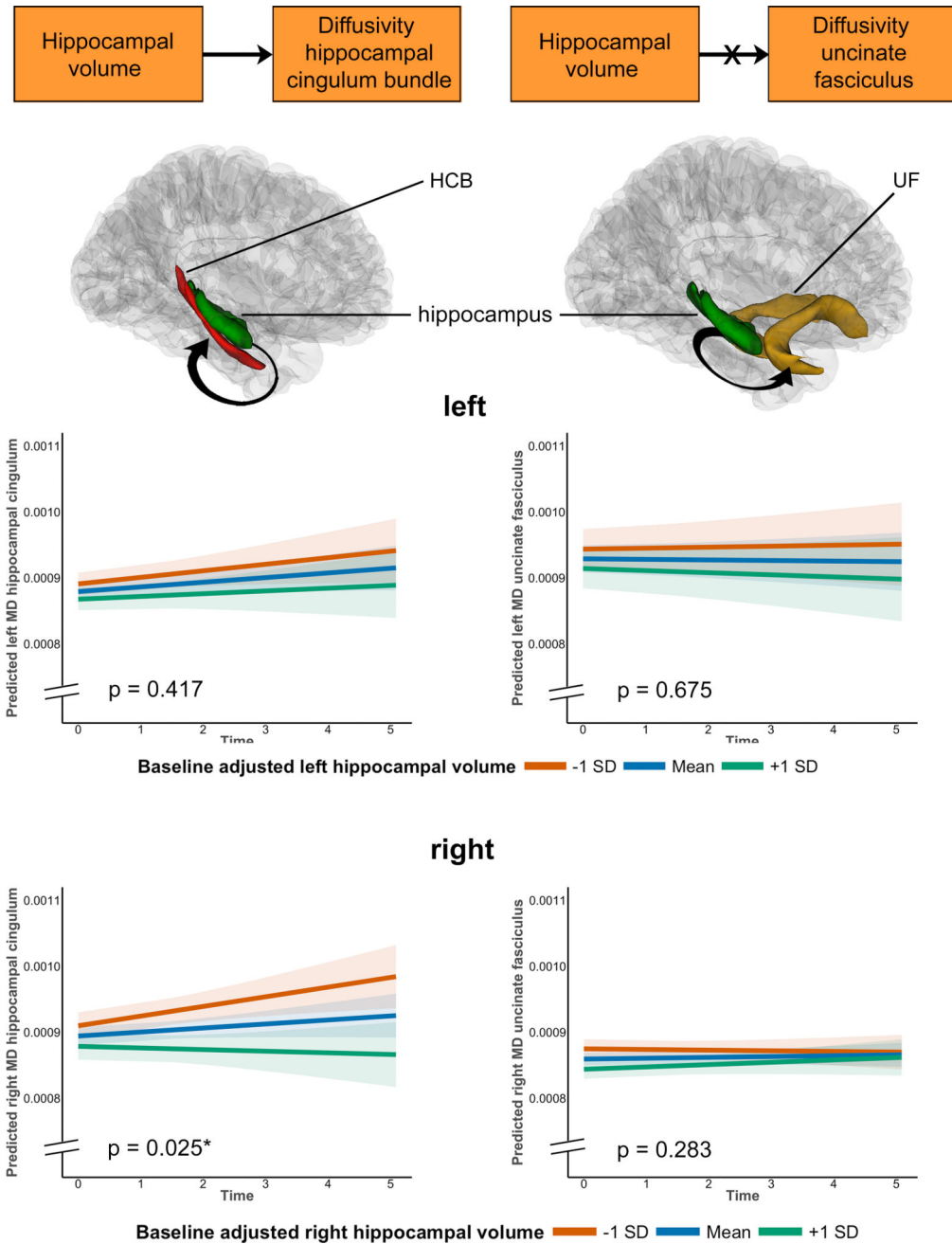


Figure 2. Associations between hippocampal volume and change in mean diffusivity in the HCB and UF

The orange boxes depict part of the model that is being investigated: we hypothesized that hippocampal volume predicts annual change in white matter diffusivity of the HCB (n= 256 unique participants) and not of the UF (n=253 unique participants). Figures below the models show the anatomical localization of the hippocampus (green), the HCB (red) and the UF (yellow) and the investigated link (arrow). The line plots (top row = left, bottom row = right hemisphere) show that right hippocampal volume predicted increased MD of the right HCB over time (left, bottom corner). No significant associations were found between hippocampal volume and changes in MD of the UF. In all line plots, estimated marginal

means of the moderation by hippocampal volume are plotted at the mean and ± 1 standard deviation, but analyses were done continuously using linear mixed effects models. Shaded areas around the fit lines show the 95% confidence interval. All p-values are two-sided and unadjusted for multiple comparisons.

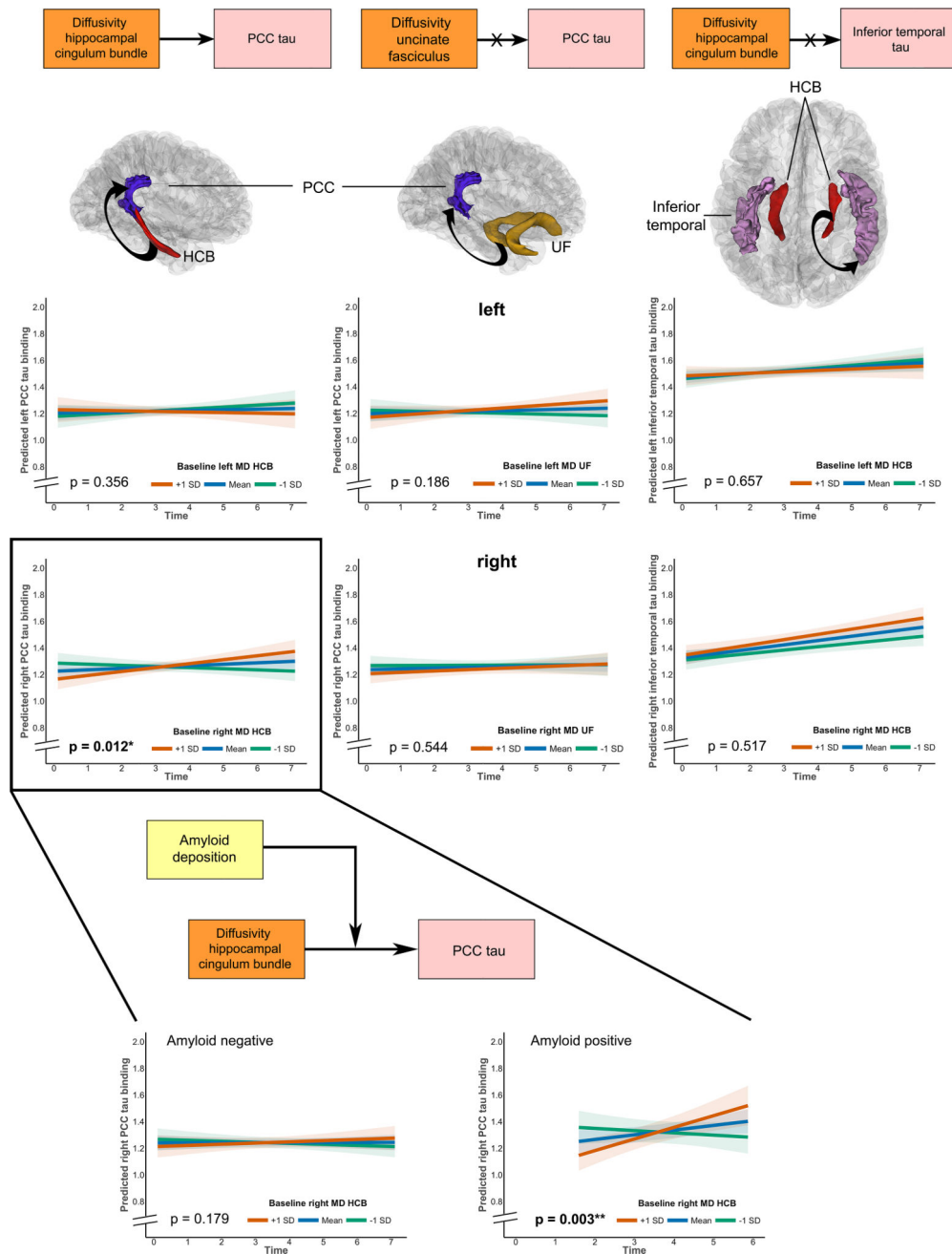


Figure 3. Associations between tract diffusivity and tau accumulation in the PCC or inferior temporal

The orange/pink boxes depict part of the model that is being investigated as depicted in Figure 1 (tract diffusivity predicting annual change in tau binding). The first column depicts first the anatomical localization of the HCB (red), the PCC (blue) and the investigated link (arrow). The line plots (top = left, bottom = right hemisphere) show that higher levels of MD in the right HCB predicted increased PCC tau accumulation (bottom left, in the black box, n=141 unique participants). The middle column shows the associations between the control tract, UF (yellow) and the PCC (blue). No significant associations were found for left or right, consistent with our hypothesis (n=139 unique participants). The right column shows

the associations between the HCB (red) and the control tau region (IT cortex). No significant associations were found for left or right (n=141 unique participants). The zoomed in section at the bottom shows the link between amyloid pathology, tract diffusivity and annual change in PCC tau accumulation (model depicted in the boxes). The line plots show that the association between right HCB diffusivity and right PCC tau change is only found in amyloid positive individuals (right, n=36 unique participants) and not amyloid negative individuals (left, n=103 unique participants). In all line plots, time was defined at the time since the baseline MRI measurement and MD of the tracts is depicted in mean \pm 1 standard deviation, but analyses were done continuously using linear mixed effects models. Shaded areas around the fit lines show the 95% confidence interval. All p-values are two-sided and unadjusted for multiple comparisons.

Abbreviations: HCB = Hippocampal cingulum bundle, UF = uncinate fasciculus, PCC = Posterior cingulate cortex

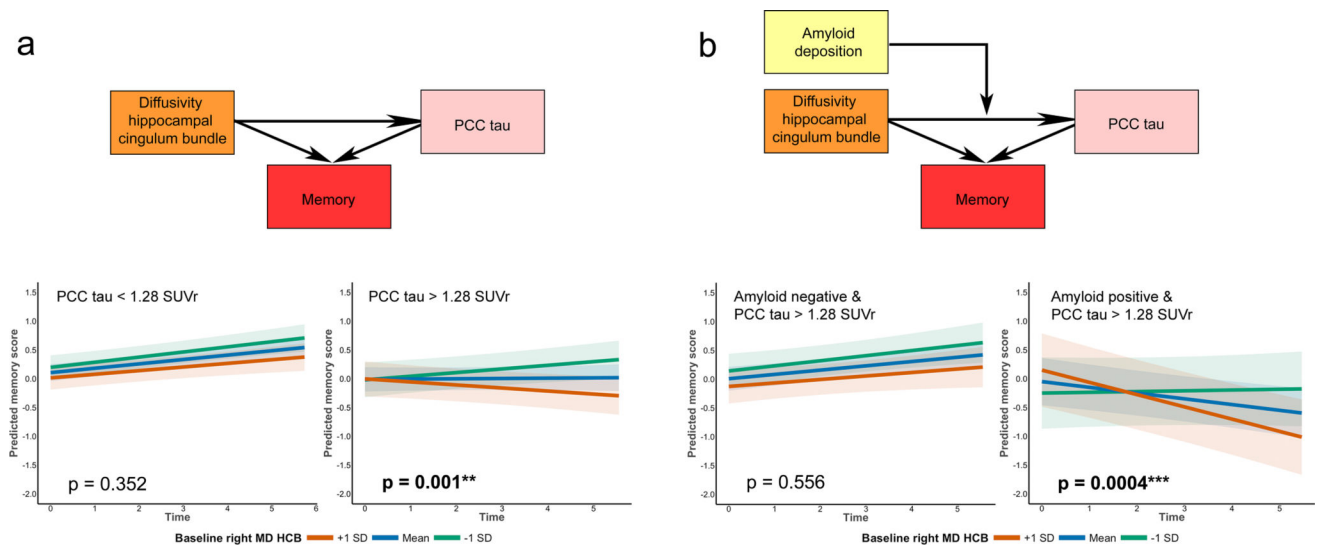


Figure 4. Associations between tract diffusivity, tau accumulation in the PCC, amyloid pathology and memory performance

The colored boxes depict part of the investigated model in Figure 1. The line plots show the breakdown of the estimates from linear mixed models examining changes memory performance predicted by hippocampal cingulum tract diffusivity in low tau (left a, $n=93$ unique participants) and high tau (right a, $n=48$ unique participants) individuals. Panel b investigated the associations between right hippocampal cingulum diffusivity and memory performance in individuals with high PCC tau who either were amyloid negative ($n=30$ unique participants) or positive ($n=18$ unique participants). The plots show a significant change in memory in individuals with high PCC tau and high amyloid levels ($n=18$, right b). In all line plots, HCB MD is depicted in mean \pm 1 standard deviation, but analyses were done continuously using linear mixed effects models. Shaded areas around the fit lines show the 95% confidence interval. All p-values are two-sided and unadjusted for multiple comparisons. Abbreviations: HCB = Hippocampal cingulum bundle, PCC = Posterior cingulate cortex, SUVr = Standardized uptake value ratio.

Table 1

Characteristics of amyloid negative and amyloid positive individuals at baseline

	Amyloid negative (n=183)	Amyloid positive (n=61)	Group difference	
			t / χ	P (unadjusted)
Age (years)	73.48 (6.23)	75.62 (6.16)	-2.34	0.021 *
Education (years)	15.62 (3.20)	16.34 (2.81)	-1.68	0.097
Sex (Female, n (%))	110 (60.11%)	37 (60.66%)	0.01	0.940
<i>APOE</i> + (n, %) [^]	33 (21.29%)	29 (53.70%)	20.64	5.541e-06 ***
MMSE (score)	29.04 (1.08)	28.85 (1.08)	1.17	0.247
Memory factor score	-0.037 (0.75)	-0.035 (0.73)	-0.02	0.987
PiB - PET levels (DVR)	1.085 (0.05)	1.421 (0.15)	-17.72	2.2e-16 ***
Left hippocampal volume	3680.64 (451.37)	3533.08 (484.21)	2.10	0.039 *
Right hippocampal volume	3791.47 (404.59)	3639.10 (468.65)	2.27	0.025 *
Left HCB, FA	0.354 (0.03)	0.353 (0.03)	0.28	0.784
Right HCB, FA	0.348 (0.03)	0.346 (0.04)	0.46	0.648
Left HCB, MD ^{\$}	0.879 (0.10)	0.887 (0.10)	-0.53	0.598
Right HCB, MD ^{\$}	0.890 (0.11)	0.911 (0.13)	-1.14	0.256
Left PCC tau (SUVr) [#]	1.192 (0.16)	1.301 (0.20)	-2.91	0.005**
Right PCC tau (SUVr) [#]	1.242 (0.16)	1.309 (0.19)	-1.93	0.059

Mean and standard deviations (or n and % for dichotomous variables) are provided. Two-sided Welch t-tests were used to calculate group differences for the continuous variables and chi-square for comparing proportions across both groups. Hippocampal volumes are adjusted for intracranial volume.

Abbreviations: MMSE = Mini-Mental State Examination, PiB = Pittsburg Compound B, DVR = dynamic volume ratio, HCB = Hippocampal cingulum bundle, FA = Fractional Anisotropy, MD = Mean Diffusivity. CI = Confidence interval;

* p < 0.05;

*** p < 0.001,

[#] tau binding levels are from the first tau PET measurement (103 amyloid negative; 36 amyloid positive individuals),

[^] Missing data for *APOE* e4 status for amyloid negative (n=28) and amyloid positive (n=7) individuals,

^{\$} MD measures were multiplied by 1000. Axial and Radial diffusivity values correlated with the MD measurements at r = 0.96 and r = 0.99 respectively.